Phase-shift modelling for HTI media

R. K. Sharma and R. J. Ferguson

ABSTRACT

Fractures play an important role in hydrocarbon production as they determine the pathways and volume of crustal fluid movement. The horizontal transverse isotropic (HTI) is the simplest effective model of a formation that contain a single fracture system. By following the same theory as discussed in paper entitled "*9C-3D* modelling for VTI media", we present phase shift modelling in order to seek the dynamic and kinematic signature of the seismic waves in HTI media as these analysis can be useful for fracture analysis. The only difference in this case resides on the way of computing the polarization angle of the incident body waves at each grid point of the interface. Consequently, a layer of infinitesimal thickness above the HTI media is taken into account conducive to define the initial wavefield propagation direction. The incident wavefield propagation direction is governed by the cross product of the unit normal vector in the direction of propagation with unit normal vector associated with rotation-symmetry axis. This cross-product yields the effective ray parameter that is the prerequisite for obtaining vertical slowness of the refracted wave in the HTI media. On being acquainted with the effective ray parameter and the vertical slowness of the refracted wave in HTI media, the unit normal vector in propagation direction in HTI media is computed and used in the cross-product of it with the unit normal vector associated with a $3C$ geophone at a grid location. This cross-product leads to the computation of polarization angle of propagating body waves in HTI media at the interface and nurture to the rotation matrix. Therefore, the rotation matrix, build on bases of the polarization angle and azimuth, is applied on the extrapolated wavefield in order to model $9C$ data. It is observed that the amplitude and travel time of seismic waves are affected by HTI medium. The presented *9C-3D* modelling will contribute to fracture detection from the surface seismic data since the information about the fracture system can be extracted from the three dimensional behavior of the shear wave splitting. Subsequently, this modelling will be applicable for VSP and micro-seismicity modelling in the presence of anisotropy.

INTRODUCTION

For recent years, Geo-scientist are supposed to explore the different kind of hydrocarbon reservoirs in behalf of increasing demand of oil and gas in the world. Many of the reservoirs, such as carbonates, tight clastic and basement reservoirs, contain a finite population of natural fractures (Zheng, 2006). Further, fractures control the fluid flow rate, which depends on the permeability of the reservoir as it's high in the direction of fractures strike and low across it (Larry, 2004). Consequently, the knowledge of the distribution of the fracture system to Geo scientist and reservoir engineers is the prerequisite for the successful development of these reservoirs. According to geology, a fracture is characterized by a planar discontinuity in rock due to deformation or physical diagenesis (Xiang-Yangi, 1997). The pattern of the fractures depends on the present and history of the stress and it is evident that certain small-scale fractures may be stress aligned and behave as anisotropic media for seismic waves with sufficiently long wavelengths (Peter and Crampin, 1990). These fractures, either having been initially open due to the stress field within Earth at present

time or subsequently closes due to mineralization, are important for fluid flow. Since open fractures can provide storage space and passage for flow of oil and gas, they are of interest for hydrocarbon exploration . There are two ways: direct and indirect, to measure fractures. Direct measurement is based on the well-logging or core sampling and has its limitation as it's applicable around well bores. Thus, indirect measurements are required to delineate fractured reservoir and to optimize the development of the reservoir. Since in most circumstances in depth in-situ fractures are more or less vertical, the simplest effective model of a formation containing a single fracture system is transversely isotropic with a horizontal symmetry axis (HTI) and is considered presently. Figure 1 shows the HTI model induced by vertical fractures where x axis is the axis of symmetry. The plane which possesses the axis of symmetry is known as symmetry axis plane and a plane normal to the symmetry axis plane is characterized by the isotropy plane and these both planes are shown in Figure 1. For present day geophysics, the crustal fracture content, distribution and possible alignment is the important subject in despite of the complexity of crustal anisotropy and if we are to comprehend the role of fractures and fluids to monitor hydrocarbon reservoirs for the presence or absence of major fluid pathways, we must understand how seismic waves interact with the fractures and how this interaction can provide an opportunity to extract the fracture information from seismic waves by considering the kinematic and dynamic analysis. In order to accomplish this purpose it's worth to review the wavefield propagation in the transverse isotropic media.

WAVE PROPAGATION IN THE TRANSVERSE ISOTROPIC MEDIA

Dealing with anisotropy in the oil and gas industry contains the two main objectives at exploration and field development stages. In exploration, we would like to improve velocity model by estimating anisotropy from available seismic data and migrate the data using this model in a hope to improve the image of target horizons compared to the image obtained by using best isotropic velocity model (Grechka, 2009). As long as it happens our job is done and we don't care about the physical reason of anisotropy. While, we do want to find out the physical reason for the measured anisotropy at field development stage. In consequence, a sound understanding of the basic principles of seismic wave propagation in anisotropic media and the ability to model the main characteristics of propagating waves are required. The equation of motion for transverse isotropic solid can be represented as

$$\rho \frac{\partial^2 u_i}{\partial t^2} = \frac{\partial \tau_{ij}}{\partial x_j}, \tag{1}$$

where the u_i are the components of particle displacement,the τ_{ij} are the stresses and ρ is the density of the corresponding medium and i, j=1, 2, 3.
To solve the equation 1 in a unique fashion, the displacement vector **u** and the stress tensor τ are related to each other as given by Hooke's law and can be expressed as

$$\tau_{ij} = c_{ijkl}\epsilon_{kl}, \tag{2}$$

where **c** is the fourth-rank stiffness tensor and $\epsilon_{ij}=\frac{1}{2}(\partial u_i/\partial x_j + \partial u_j/\partial x_i)$, and i, j=x, y, z or 1, 2, 3. The substitution of the equation 2 into equation 1 yields the wave equation as

$$\rho \frac{\partial^2 u_i}{\partial t^2} = c_{ijkl}\frac{\partial^2 u_k}{\partial x_l \partial x_j}. \tag{3}$$

Azimuthal Anisotropy (HTI)
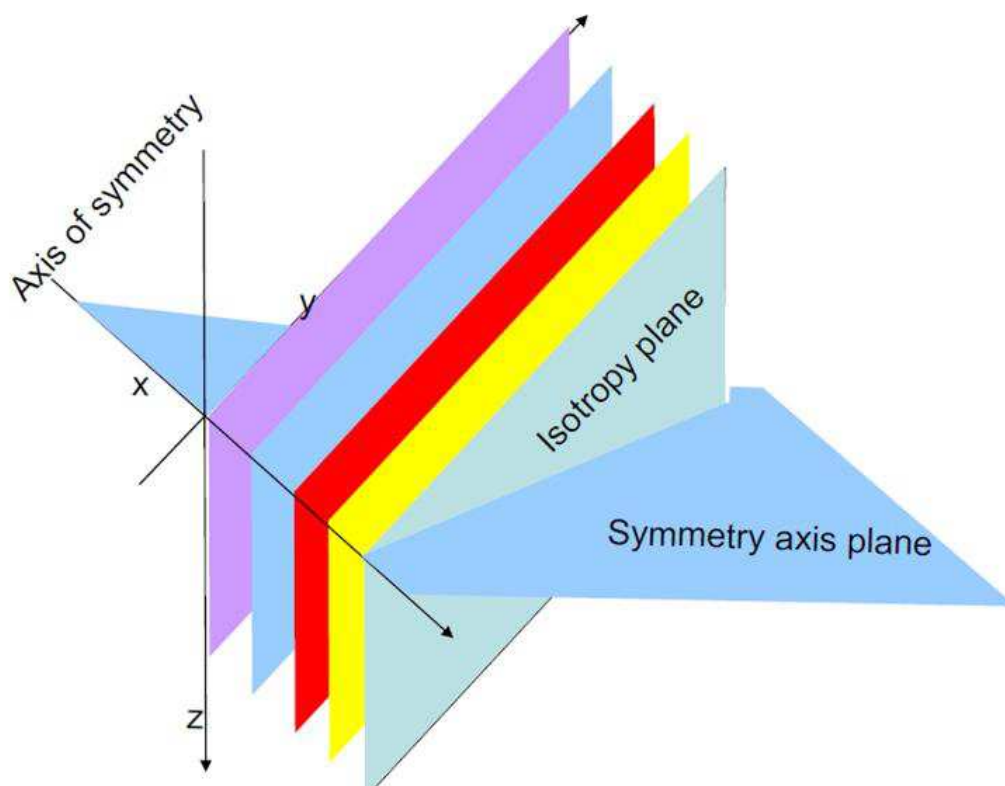
FIG. 1: Schematic representation of HTI medium induced by vertical fractures where x axis is the axis of symmetry. The plane which possesses the axis of symmetry is known as symmetry axis plane and a plane normal to the symmetry axis plane is characterized by the isotropy plane (Nadri, 2009).

Its standard solution is a harmonic plane wave of form

$$u_k = AU_k e^{i\omega(n_j x_j/V - t)}, \tag{4}$$

where $\mathbf{U}$ is the polarization vector, ω is the angular frequency, $\mathbf{n}$ is the unit wavefront normal and V is the phase velocity. Substitution of the plane wave solution 4 into the equation 3 leads to the Christoffel equation (Tsvankin, 2001)

$$\begin{bmatrix} G_{11} - \rho V^2 & G_{12} & G_{13} \\ G_{21} & G_{22} - \rho V^2 & G_{23} \\ G_{31} & G_{32} & G_{33} - \rho V^2 \end{bmatrix} \begin{bmatrix} U_1 \\ U_2 \\ U_3 \end{bmatrix} = 0. \tag{5}$$

with $G_{ik} = c_{ijkl} n_j n_l$.

The Christoffel equation 5 is the most important equation for analysis of wave phenomena in anisotropic media. In fact this equation is treated as eigenvalue-eigenvector problem for the symmetric, positive definite matrix $\mathbf{G}$. The positive definiteness of tensor $\mathbf{c}$ ensures the positive definiteness of $\mathbf{G}$ while its symmetry is the consequences of the symmetry of the stiffness tensor. Since the kinematic and dynamic signature of body waves for HTI media can be obtained from known analysis of VTI media, we consider a transverse isotropic medium and z axis coincide with the normal to the plane of transverse isotropy and can be treated as axis of rotation-symmetry. However, it's known that such a media can be characterized by five elastic constant (Slawinski, 2003) and using these constants in equation 5, the eigenvalues of the Christoffel equation can be obtained from

$$det[G_{ij} - \rho V^2 \delta_{ik}] = 0, \tag{6}$$

which yields a cubic equation for ρV^2. The Christoffel equation yields three possible values of the phase velocity which belongs to P-wave and two shear waves for a given phase direction $\mathbf{n}$. Therefore, the S-wave is splitted into two modes with different velocities and polarizations. However, the three eigenvalues of $\mathbf{G}(\mathbf{n})$ are the squared phase velocities of three body waves and can be expressed as

$$V_p^2(\theta) = \frac{1}{2\rho}[(c_{11} + c_{44})\sin^2(\theta) + (c_{33} + c_{44})\cos^2(\theta) + D], \tag{7}$$

$$V_{sv}^2(\theta) = \frac{1}{2\rho}[(c_{11} + c_{44})\sin^2(\theta) + (c_{33} + c_{44})\cos^2(\theta) - D], \tag{8}$$

and

$$V_{sh}^2(\theta) = \frac{1}{\rho}[c_{66}\sin^2(\theta) + c_{44}\cos^2(\theta)], \tag{9}$$

where

$$D = ([[(c_{11} - c_{44})\sin^2(\theta) - (c_{33} - c_{44})\cos^2(\theta)]^2 + 4(c_{13} + c_{44})^2 \sin^2(\theta)\cos^2(\theta))^{1/2}. \tag{10}$$

The complexity of these equation is a main problem to use of anisotropic model for seismic exploration but it can be reduced by using Thomson's parameters (Thomsen, 1986). These

parameters play an important role for understanding seismic signatures in anisotropic media and can be expressed as

$$\alpha_0 = \sqrt{\frac{c_{33}}{\rho}}, \tag{11}$$

and

$$\beta_0 = \sqrt{\frac{c_{55}}{\rho}}, \tag{12}$$

where α_0, β_0 are the P-wave and S-wave velocities along the rotation-symmetry axis and anisotropy can be characterized by the dimensionless coefficients

$$\epsilon = \frac{c_{11} - c_{33}}{2c_{33}}, \tag{13}$$

$$\gamma = \frac{c_{66} - c_{55}}{2c_{55}}, \tag{14}$$

and

$$\delta = \frac{(c_{13} + c_{55})^2 - (c_{33} - c_{55})^2}{2c_{33}(c_{33} - c_{55})}. \tag{15}$$

The instinctive application of coefficients ϵ and γ is clear as they vanish in isotropic media. Thus, the magnitude of the P and SH-wave anisotropy can be measured from the values of ϵ and γ. The intuitive appeal of coefficient δ is not as transparent as those of ϵ and γ and might seem unexpected. The significance of δ becomes apparent once it's noticed that

$$\frac{d^2 V_p}{d\theta^2} \mid_{\theta=0} = 2\delta\alpha_0. \tag{16}$$

Consequently, δ is not just an arbitrary combination of the elastic coefficients. Instead, the curvature of the P-wave velocity function at the vertical is governed by δ. It also governs the P-wave normal moveout velocities from horizontal reflectors and plays an key role for seismic reflection data (Grechka, 2009). On being acquainted with Thomson's parameters, the phase velocity expression of the body waves can be expressed as

$$V_p^2(\theta) = \alpha_0^2[1 + \epsilon \sin^2\theta + D^*(\theta)], \tag{17}$$

$$V_{SV}^2(\theta) = \beta_0^2[1 + \frac{\alpha_0^2}{\beta_0^2}\epsilon \sin^2\theta - \frac{\alpha_0^2}{\beta_0^2} - D^*(\theta)], \tag{18}$$

and

$$V_{SH}^2(\theta) = \beta_0^2[1 + 2\gamma \sin^2\theta], \tag{19}$$

where

$$D^*(\theta) = \frac{1}{2}(1 - \frac{\beta_0^2}{\alpha_0^2})\{[1 + \frac{4\delta}{(1 - \frac{\beta_0^2}{\alpha_0^2})^2} \sin^2\theta \cos^2\theta + \frac{4(1 - \frac{\beta_0^2}{\alpha_0^2} + \epsilon)\epsilon}{(1 - \frac{\beta_0^2}{\alpha_0^2})^2} \sin^4\theta]^{1/2} - 1)\}. \tag{20}$$

Once the eigenvalues of the Christoffel equation are known as equations 17, 18 and 19, the corresponding eigenvectors $\mathbf{U}$ can be computed from any two equation of the three

equation of the Christoffel equation 5. Since the Christoffel equation is real and symmetric, the obtained polarization vectors of the body waves are mutually orthogonal for any given phase direction **n** (Tsvankin, 2001). However, the polarization are generally neither parallel nor orthogonal to the wavefront normal. Further, prior to analysis the dynamic signature of body waves in the transverse isotropic media, it's convenient to understand the difference between the group velocity and the phase velocity.

Group velocity

The group velocity-vector characterizes the direction and speed of energy associated with the wave motion, therefore, is of primary importance in seismic travel modelling and inversion methods. In contrast, the phase velocity is the local velocity with which wavefront propagates in the normal direction to it. For transverse anisotropic, the difference between the group and phase velocity vectors are caused by velocity variation with angle. As depicted in Figure 2 the group angle represents the direction of the group velocity vec-
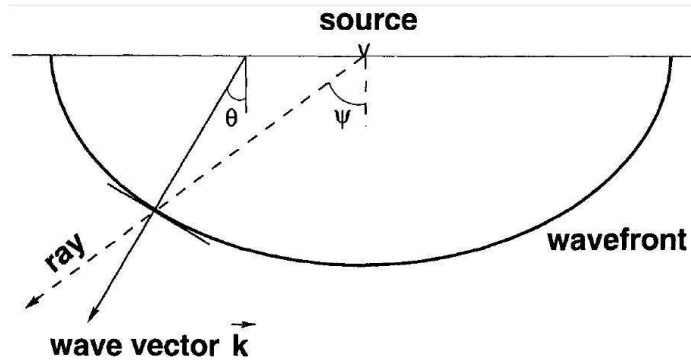
FIG. 2: Schematic representation of the phase and group angles. The angle is measured with vertical axis. The group angle depicts the direction of energy propagation while phase angle determines the direction of wavefront propagation (Tsvankin:2001).

tor in a homogeneous medium and it is aligned with the source-receiver direction while the phase angle is the angle between the wave vector $\tilde{\mathbf{k}}$ and the vertical axis. These angles are different just because of the lack of sphericity of wavefront in the presence of anisotropy. In contrast to phase velocity which can be obtained from the Christoffel equation, group velocity can be computed from the phase velocity function by using this relationship

$$V = \mathbf{g}.\mathbf{n}, \tag{21}$$

between the group and the phase velocities. Now to obtain the group velocity from the equation 21, the spatial direction of the unit wavefront normal **n** can be characterized by two directional angles θ_1 and θ_2. These angles are knowns as the polar angle and the azimuth of **n**, respectively. So the wavefront normal can be computed as

$$\mathbf{n} = [\sin\theta_1 \cos\theta_2, \sin\theta_1 \sin\theta_2, \cos\theta_1]. \tag{22}$$

The differentiation of the equation 21 leads the expression

$$\frac{\partial V}{\partial \theta_i} = \mathbf{g}.\frac{\partial \mathbf{n}}{\partial \theta_i} + \frac{\partial \mathbf{g}}{\partial \theta_i}.\mathbf{n}(i = 1, 2). \tag{23}$$

By definition, $\mathbf{n}$ is the normal to the wavefront, whereas the derivatives $\partial \mathbf{g}/\partial \theta_i$ are tangent to it. Hence, the second term on the right -hand side of above equation vanishes. Thus

$$\frac{\partial V}{\partial \theta_i} = \mathbf{g}.\frac{\partial \mathbf{n}}{\partial \theta_i}(i = 1, 2). \tag{24}$$

At this moment considering the equations 21 and 24, the component of the group velocity vector can be obtained according to expression

$$\mathbf{g} = V\mathbf{n} + \frac{\partial V}{\partial \theta_1}\frac{\partial \mathbf{n}}{\partial \theta_i} + \frac{1}{\sin^2 \theta_1}\frac{\partial V}{\partial \theta_2}\frac{\partial \mathbf{n}}{\partial \theta_2}. \tag{25}$$

This equation leads to the following conclusions

- The magnitude of the group velocity can be defined as

$$g \equiv \|\mathbf{g}\| = \sqrt{V^2 + (\frac{\partial V}{\partial \theta_1})^2 + \frac{1}{\sin^2 \theta_1}(\frac{\partial V}{\partial \theta_2})^2}. \tag{26}$$

  Therefore, the inequality $V \le g$ is satisfied by the phase and group velocities for any wavefront normal $\mathbf{n}$.

- As it's known that ray is the unit vector, $\mathbf{r}$, parallel to the group velocity so it can be defined as

$$\mathbf{r} = \frac{\mathbf{g}}{g}. \tag{27}$$

- Following the equation 21 it can be demonstrated that

$$\mathbf{r}.\mathbf{n} = \frac{V}{g}. \tag{28}$$

If $\mathbf{r} \ne \mathbf{n}$, the ray deviates from the wavefront normal towards the phase velocity increase in accordance with equation 25. Figure 3 illustrates this geometrically. From Figure 3, it's evident that

$$\cos(\theta - \psi) = \frac{V(\theta)}{V(\psi)} = \frac{V(\theta)}{g(\psi)}, \tag{29}$$

Now by considering the right triangle whose hypotenuses is $\mathbf{g}$ and V, $\partial V/\partial \theta$ are the sides, it can be illustrated that

$$\tan(\theta - \psi) = \frac{1}{V(\theta)}\frac{dV(\theta)}{d\theta}, \tag{30}$$

and the trigonometric identity

$$\tan(x - y) = \frac{\tan x - \tan y}{1 + \tan x \tan y}, \tag{31}$$

leads to the relationship between the group angle and the phase angle as

$$\psi = \tan^{-1}\left[\frac{\tan\theta + \frac{1}{V(\theta)}\frac{dV(\theta)}{d\theta}}{1 - \frac{1}{V(\theta)}\frac{dV(\theta)}{d\theta}\theta}\right].$$

(32)

According to equation 32, the equality $\psi = \theta$ occurs only when $dV(\theta)/d\theta = 0$, that is, at extrema of $V(\theta)$. At those extrema, the ray direction coincides with wavefront normal's direction and the group-and phase velocity surfaces touch each other as shown in Figure 3.
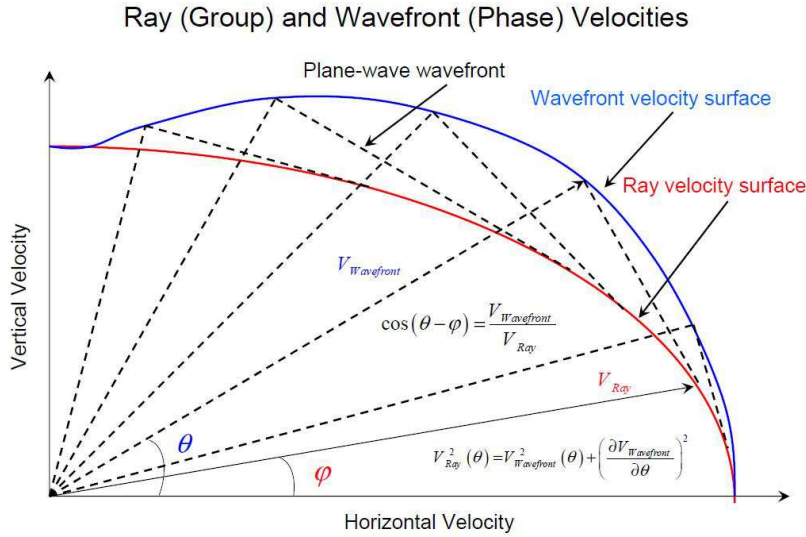
FIG. 3: Schematic representation of the relationship between phase velocity and group velocity surfaces. The angles ψ and θ are the group and phase angles, respectively and are measured with horizontal axis. It illustrates that the group velocity surface can be constructed from the known phase velocity surface. Plane-wave fronts are the normal drawn from known points of the phase velocity surface to the group velocity surface and governs the energy distribution for a given direction (Nadri, 2009).

So far we have discussed about the crucial factors which can be used in order to analyze the dynamic behavior of the body wave propagation, through the anisotropic media. Travel times in anisotropic media are accommodated through the plane wave transformation and phase shift. For accomplishing phase shift modelling we have implemented same theory as discussed by the author in another CREWES report (Sharma and Ferguson, 2010). The only difference is that a layer of infiniteness thickness above the HTI medium is taken into account here in order to define the wavefield propagation direction initially. We have implemented a constraint on this layer that the velocity possessed by it is the maximum velocity of the lower HTI media. The incident wavefield propagation direction is governed by the cross product of the unit vector normal to the plane wavefront with unit vector in the direction of axis of symmetry as

$$p_I = |\hat{\mathbf{p}} \times \hat{\mathbf{a}}| \sqrt{p_1^2 + p_2^2 + q^2},$$

(33)

where p_1, p_2 and q are the horizontal components 1, 2 and the vertical component of the slowness vector, respectively and these are evaluated in the incident medium. For HTI media presently, we take the interface characterized by ($\hat{\mathbf{a}}=\hat{\mathbf{j}}$). Once the effective ray parameter p_I is computed, the vertical slowness q_{HTI} of the incident body wave in the lower HTI media can be computed in terms of the Thomson's parameter and the effective ray parameter and are known for all the body waves (Sharma and Ferguson, 2010). On being acquainted with the effective ray parameter and the vertical slowness of the incident wavefield in the HTI media, the unit vector normal to the plane wavefront in the propagation direction can be determined as

$$\hat{\mathbf{p}}_{\mathbf{HTI}} = \frac{p_1\,\hat{\mathbf{i}} + p_2\,\hat{\mathbf{j}} + q_{HTI}\,\hat{\mathbf{k}}}{\sqrt{p_1^2 + p_2^2 + q_{HTI}^2}}. \tag{34}$$

Now, the cross product of this unit vector with the vertical axis of a $3C$ geophone

$$\left| \mathbf{p}\hat{}_{HTI} \times \hat{\mathbf{a}} \right|, \tag{35}$$

yields the polarization angle at each *3C* geophone located at the interface and nurture to the rotation matrix as the knowledge of the polarization angle is the essential parameter for obtaining rotation matrix. Once rotation matrix is build, it is implemented on the extrapolated wavefield in order to model *9C-3D* data.

EXAMPLE

We consider a homogeneous and anisotropic HTI medium of 700 m thickness for a simple demonstration. The fact that the ratio of fracture size to the seismic wavelength less than 1 makes the medium to be effectively homogeneous and anisotropic. Further, Thomson's parameters are considered from Vernik's paper for the medium characterization. Now a known impulsive source is extrapolated through the medium in plane wave domain and transformed back into the space and time domain at interface. Prior to energy distribution among the three components of the *3C* geophones, we consider the in-line, cross-line and time slices of the known extrapolated wavefield in order to analyze the kinematic and dynamic behavior of the body waves in the HTI media. Presently, the in-line and cross-line directions are characterized by the fracture's strike direction and normal to it, respectively. Consequently, first a known P-wave source is considered at the earth surface and is extrapolated through the HTI medium. Figure 4a shows the in-line slice of the extrapolated wavefield and the cross-line slice is shown in the Figure 4b. Kinematically, these slices lead to the following observations

- The arrival time of the extrapolated wavefield at zero offset is same in the in-line slice as well as in the cross-line slice.

- The travel time response of the in-line slice is hyperbolic while is non-hyperbolic of the cross-line slice.

- The arrival time of the extrapolated wavefield at far offset in the in-line slice is less than register in the cross-line slice. It is a manifestation of the well known fact that the P-wave travel fast in the direction of fracture strike and slow in the direction normal to it.

Figure 5a and b show the time slices of the extrapolated wavefield without and with analytic curve. The obtained ellipse in the $x - y$ plane manifests the azimuthal anisotropy of the medium as expected. The overlapping of the analytic ellipse with the obtained one ensures the accuracy of the proposed phase shift modelling, kinematically.
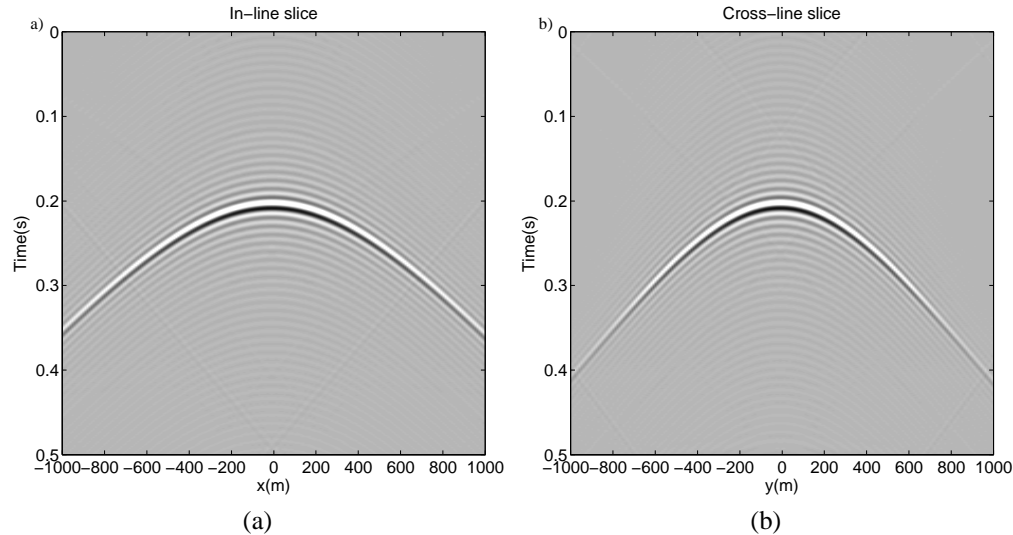
FIG. 4: (a) In-line (b) Cross-line slices of the extrapolated P wavefield through an anisotropic medium characterized by Thomson's parameters shown in appendix. The considerable difference between these slices is observed kinematically as well as dynamically. Both slices manifest well known fact that P-wave travel fast in the direction of fracture's strike with high amplitude.

Dynamically, it is noticed that P-wave amplitude increases from the slow direction to the fast direction. This observation correlates well with the equation 28 and Figure 3 where it is mentioned that ray deviates towards the high phase velocity direction from the low velocity direction in the presence of anisotropy. In addition to this, if we draw a normal from a known point of the phase velocity surface to the group velocity surface, the point where it makes a contact with the group velocity surface corresponds to the plane wave drawn tangentially at that point. Then the energy distribution depends on how close these points are at the group velocity surface and it can be observed from the Figure 3 that these points are dense in and near the fast velocity direction while sparse in the low velocity direction and hence the observed amplitude pattern in our analysis. Now, in order to seek the influence of the anisotropy on the kinematic and dynamic behavior of the P-wave we are repeating the same procedure as outlined above after introducing the different anisotropy in the same model as taken previously. Figure 6a and b show the in-line and the cross-line slices of the extrapolated wavefield for the same medium as before but for a positive value of δ. The time slices of the extrapolated wavefield with and without analytic curve are shown in Figure 7a and b. In continuation of this analysis, the in-line and the cross line slices for negative δ are shown in the Figure 8a and b and the time slices are shown in the Figure 9a and b. A close examination of these figures make it possible to illustrate the following observations

- Kinematically, the different values of the δ do not have any effect on the in-line
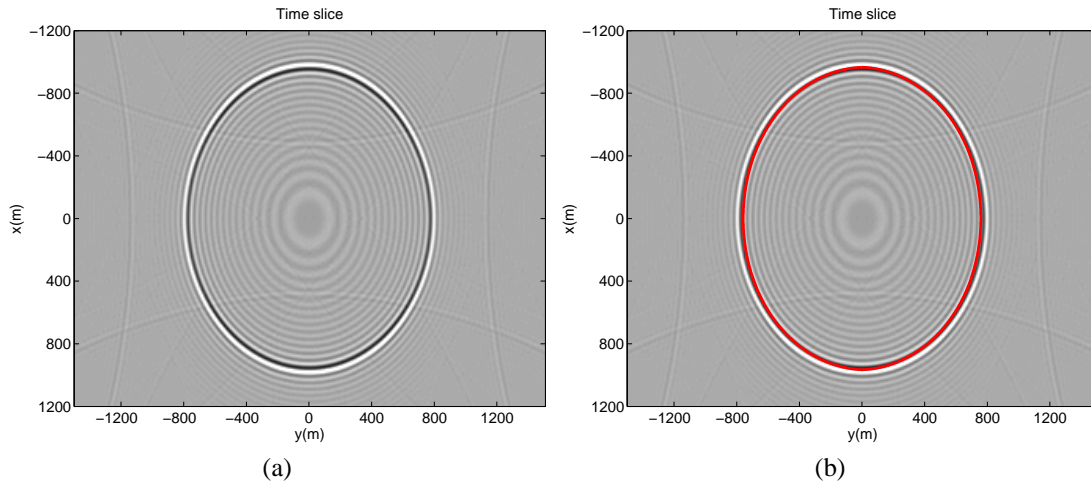
FIG. 5: Time slices of extrapolated P wavefield (a) without (b) with analytic curve. Obtained ellipse is a manifestation of azimuthal anisotropy as expected. More energy is observed in fast direction. The overlapping of the analytic curve (shown in red color) with the obtained ellipse illustrates authentication of proposed phase shift modelling.
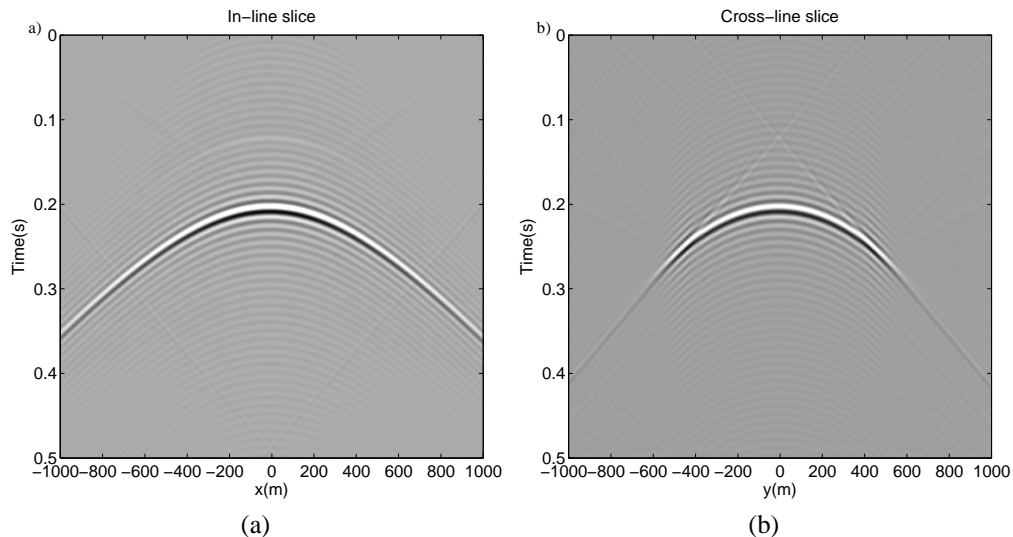
FIG. 6: (a) In-line (b) Cross-line slices of the extrapolated P wavefield for same model as before but for a larger magnitude of anisotropy (higher δ=0.29) in the medium. The large value of δ does have effect on the cross-line slice while the in-line slice is not influenced.
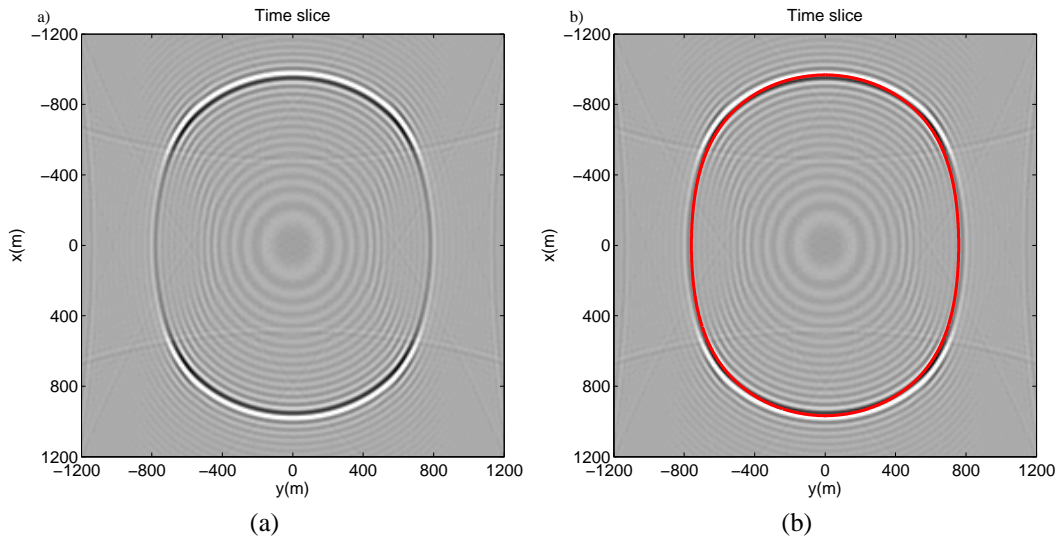
FIG. 7: Time slices of the extrapolated P wavefield (a) without (b) with analytic curve. The large value of δ does have influence on the kinematic and dynamic behaviors of P-wave.
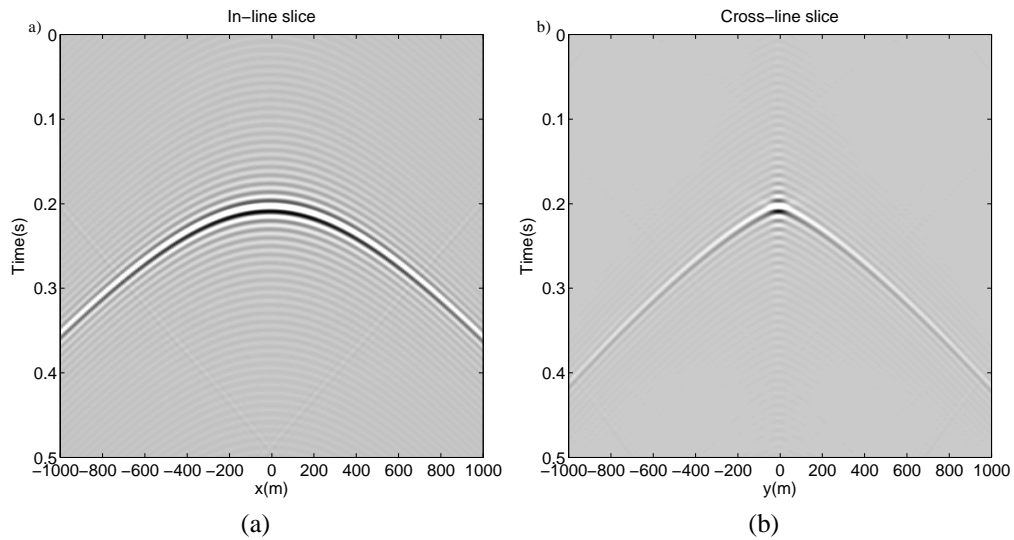
FIG. 8: (a) In-line (b) Cross-line slices of the extrapolated P wavefield for the same model as considered for above Figure but for large negative value of δ (δ=-0.2). A considerable effect, kinematically as well as dynamically, of anisotropy is observed on the cross-line slice.
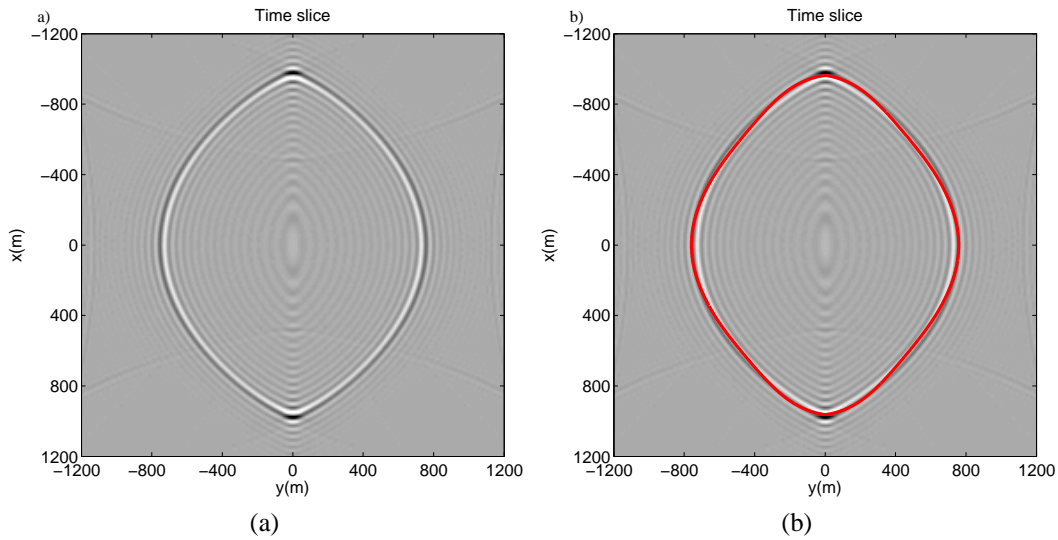
FIG. 9: Time slices of the extrapolated P wavefield (a) without (b) with analytic curve for the same medium as considered in Figure 8. The authentication of the proposed modelling is demonstrated here as analytic curve is analogous to the obtained one.
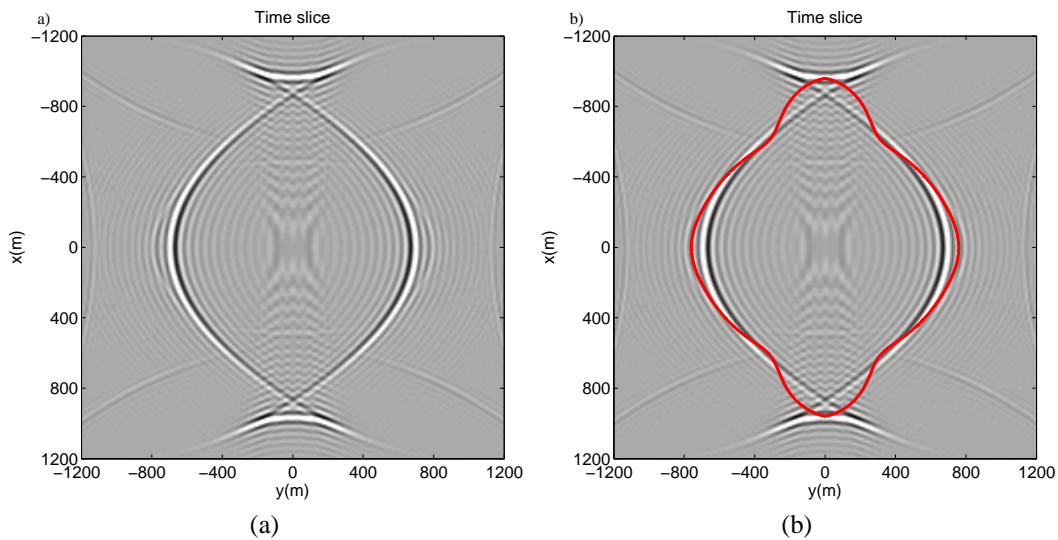
FIG. 10: Time slices of the extrapolated P wavefield (a) with (b) without analytic curve through the medium characterized by Thomson's parameters chosen randomly. The unexpected behavior, kinematically and dynamically, illustrates that choice of Thomson's parameters for a medium characterization can not be random.

slice's response while do have the noticeable effect on that of the cross-line slice. The authentication of the proposed phase shift modelling is shown in these figures as analytic ellipse coincides with the obtained ellipse.

- Dynamically, at a given time the energy distribution in the $x - y$ plane depends on the magnitude of the anisotropic parameter δ. Further, it's noticed that for negative δ the contrast in the in-line and cross-line's energy is more than that for the positive δ.

Moreover, the choice of the δ for the figures shown above was limited on the behalf of the relationship between elastic stiffness constants and Thomson's parameters as shown in appendix. Thus, the adopted value of δ should make physical sense and can not be taken randomly and it can be verified in reference of Figure 10 . Figure 10a and b show the time slice of the extrapolated wavefield for the delta chosen randomly. It is observed here that the maximum amplitude of P-wave occurs in the slow direction and decreases towards the fast direction and there is no overlapping of analytic and the obtained ellipses. Thus, the demonstrated dynamic behavior of the propagated P-wave is just opposite what we expected and make it necessary that the selection of δ can not be random.   Figure
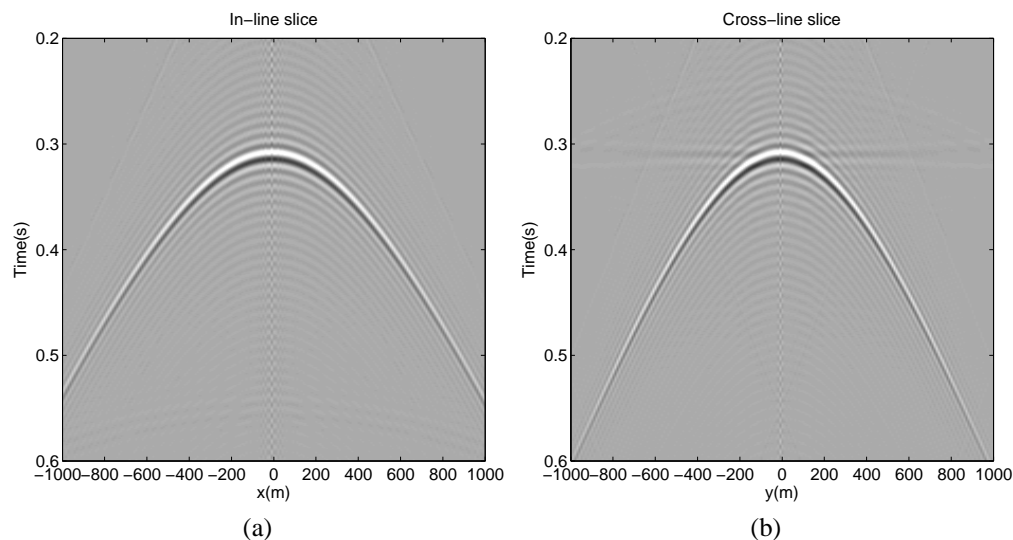
FIG. 11: (a) In-line (b) Cross-line slices of the extrapolated SH wavefield for same model as considered in Figure 4 with low resolution. The difference, kinematically or dynamically, can be examined precisely on behalf of these slices.

11a and b show in-line and cross-line slices of the extrapolated SH-wave through the same model as considered in Figure 4. Both of these slices are plotted with with a high clipped display, otherwise, the difference in between these slices in terms of amplitude and travel time would not be noticeable. Although, It is observed from Figure 12a that SH-wave travel fast in direction of fracture's strike and energy decreases from the fast direction to the slow direction and follow the same behavior as of P-wave. Kinematically, the authentication of the proposed modelling for SH-wave in anisotropic medium is demonstrated as analytic curve (shown in magenta color) matches with obtained one in Figure 12b. Again, to observe the influence of anisotropy on the kinematic and dynamic behaviors of SH-wave, the same model as considered for Figure 11, is taken into account after introducing large anisotropy
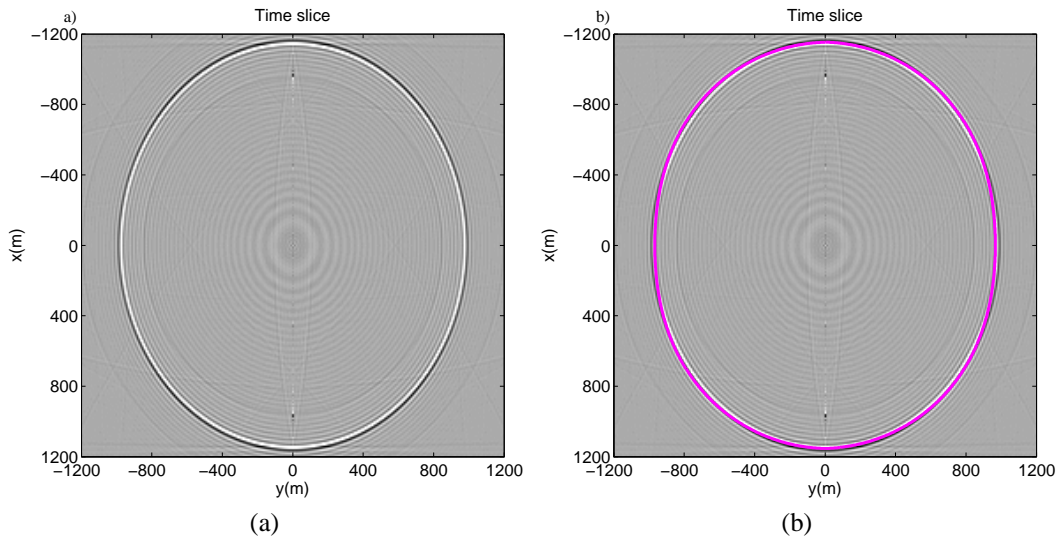
FIG. 12: Time slices of the extrapolated SH wavefield (a) without (b) with analytic curve for same medium as ones shown in Figure 11 and demonstrate that SH-wave travel fast in direction of fracture's strike with high amplitude and illustrate the authentication of the proposed modelling.

(higher γ) into the medium through which SH-wave propagates ($\gamma = 0.34$). The in-line and the cross-line slices are shown in Figure 13a and b. The dissimilarity between these two slices is observed here in terms of travel time and amplitude. However, these analysis can be emphasized in reference to Figure 14a where it is demonstrated that more energy travel in fast direction. As this Figure differs from the Figure 12a it is possible to make a conclusion that anisotropy does have effect on kinematic and dynamic behaviors of the SH-wave. So far, we have discussed about the effect of anisotropy on wavefield propagation of seismic waves. Now following the same theory as outlined above through equation 33 to 35 we have obtained *3C* data for known P-wave source at surface after applying the rotation matrix on the extrapolated wavefield and have taken slice through the in-line direction and shown in Figure 15. The red dashed line highlighted in the circle at the top right corner of Figure 15c indicates the direction along which a vertical slice of the modelled data is taken. The in-line and cross-line directions are indicated by blue and magenta color, respectively. Figure 15a, b and c show the registered energy versus offset (REVO) analysis of P-wave on H_1, H_2 and V components while registered energy versus azimuth (REVA) analysis is shown in Figure 16a, b and c, respectively. Moreover, these figures follow the expected pattern of registered energy on the different components with offset and azimuth.

SV-case

Now the same theory as discussed above has been implemented for SV-wave. In order to analysis the kinematic and dynamic behavior of the SV-wave in HTI medium, the same model as used for P and SH-wave is considered. Figure 17a and b show the in-line and cross-line slices of the extrapolated SV wavefield. It is observed that both of these slices are very close to each other in terms of travel time response. Figure 18a and b illustrate time slices of the extrapolated wavefield. The obtained circle indicates that anisotropy does
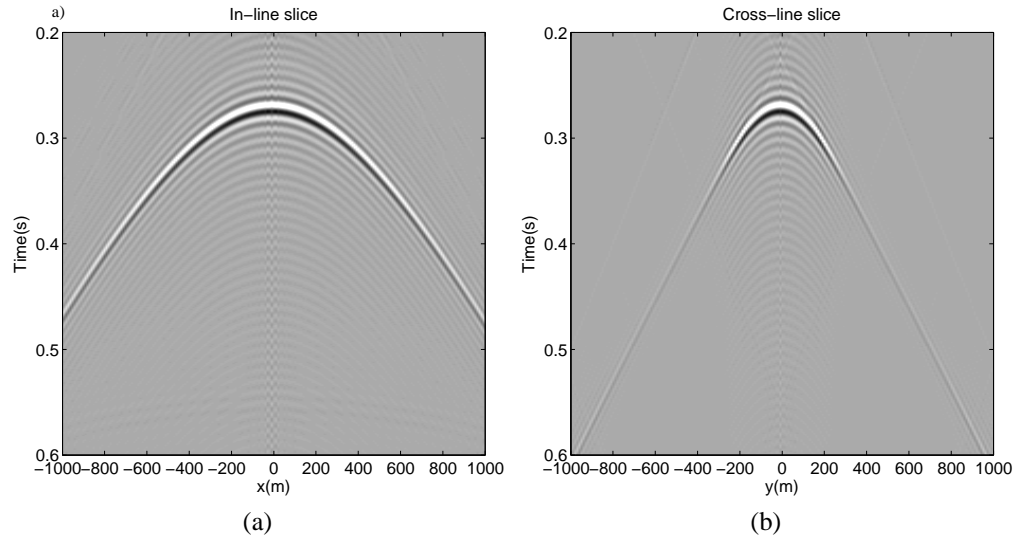
FIG. 13: (a) In-line (b) Cross-line slices of the extrapolated SH wavefield for the same model as considered above but of large anisotropy ($\gamma = 0.34$) and show the effect of anisotropy on propagation of the SH wavefield.
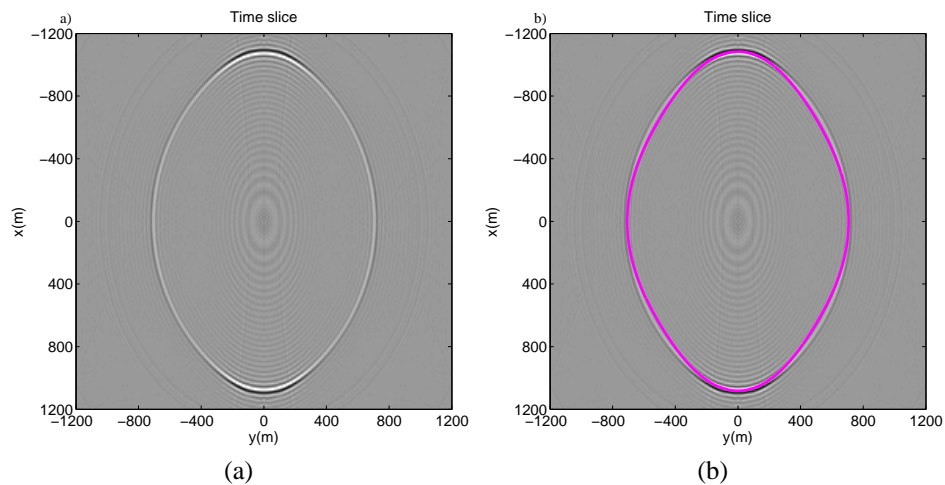
FIG. 14: Time slices of the extrapolated SH wavefield through the same model as ones shown in Figure 13. The authentication of the proposed modelling is shown in (a) and (b) kinematically and dynamically, respectively.
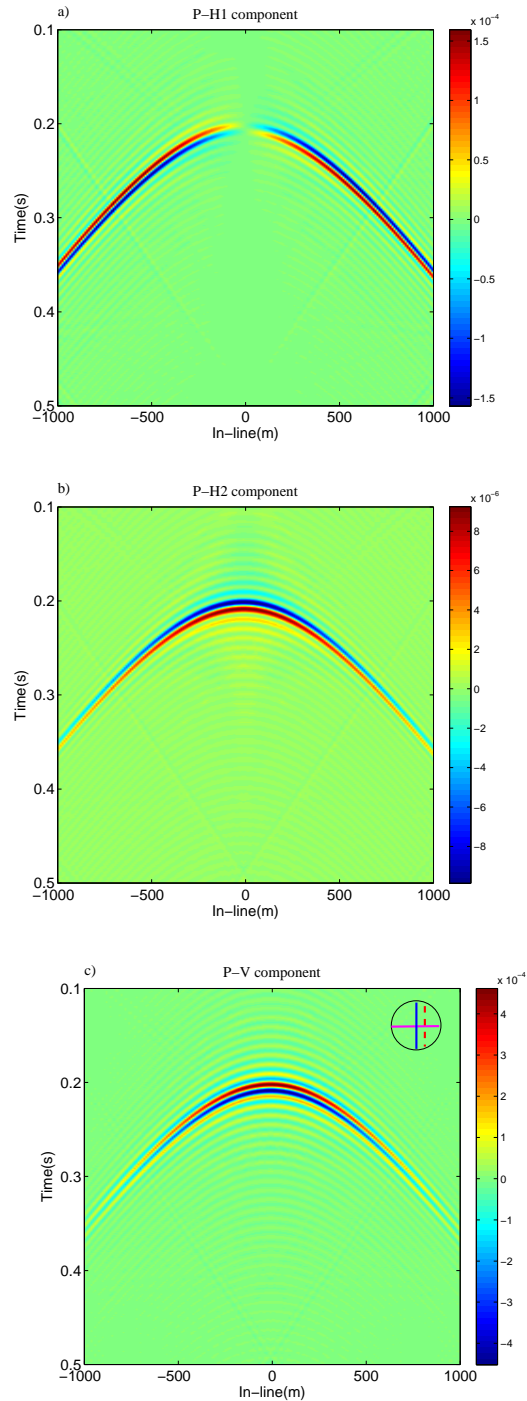
FIG. 15: (a) Registered energy versus offset (REVO) analysis of P-wave on H1 component illustrate that H1 component is more favorable for energy registration as offset increases. Polarity reversal appear on the either side of zero offset. (b) (REVO) analysis of P-wave on H2 component illustrate that H2 component is more favorable for energy registration near to zero offset. Polarity remains stationary on the either side of zero offset. (c) Recorded P-wave energy on vertical component demonstrate that energy registration on vertical component decreases with offset. Polarity follow the stationary behavior on either side of zero offset.
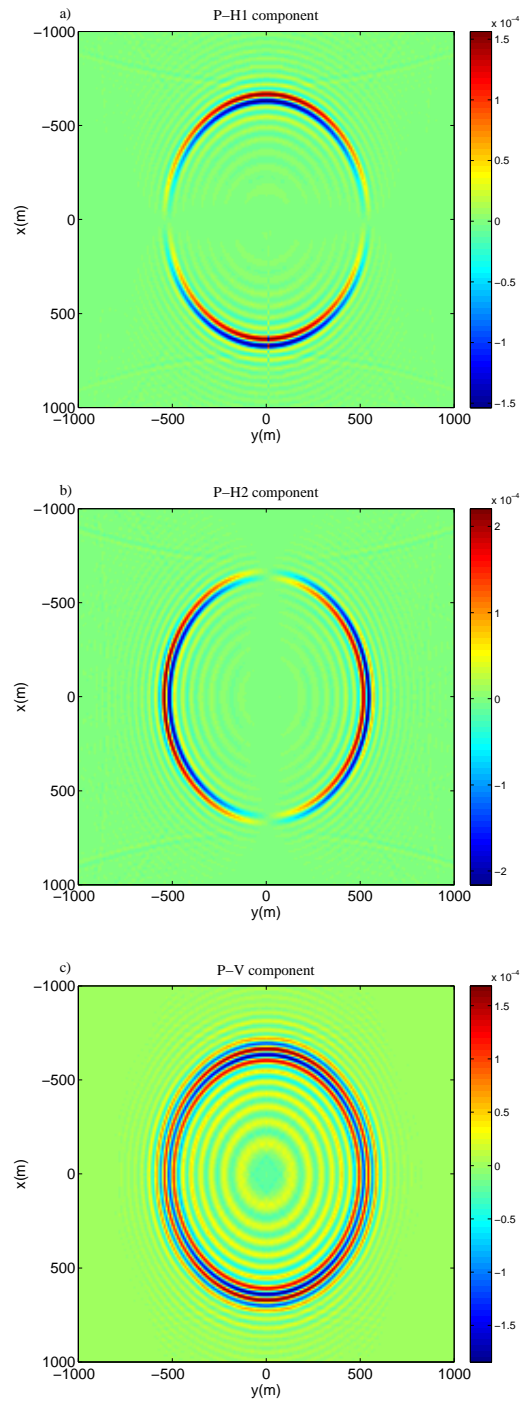
FIG. 16: (a) Registered energy versus azimuth(REVA) analysis of P-wave at H1 compo-
nent indicates that energy registration increases as azimuth increases from 0 to 90. Polarity
reversal occur on the either side of a line that bisects the circle along cross-line direction.
(b) REVA analysis of P-wave at H2 component indicates that energy registration decreases
as azimuth increases from 0 to 90. Polarity reversal occur on the either side of a line that bi-
sects the circle along in-line direction. (c) REVA analysis of P wave on vertical component
reveal the variation of recorded energy and polarity with azimuth.

not have a such considerable effect on SV-wave propagation as had on P and SV-wave propagations for this case. Further, the effect of anisotropy on the SV-wave propagation has been examined on behalf of considered model shown in appendix. Figure 19a and b
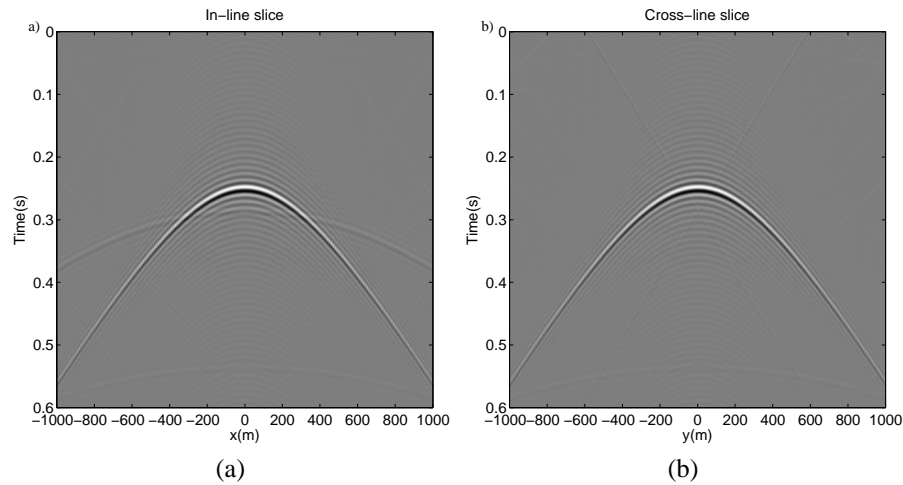
FIG. 17: (a) In-line (b) Cross-line slices of the extrapolated SV wavefield for the same model as considered above for P- and SH-waves. The in-line slice is analogous to the cross-line slice
.
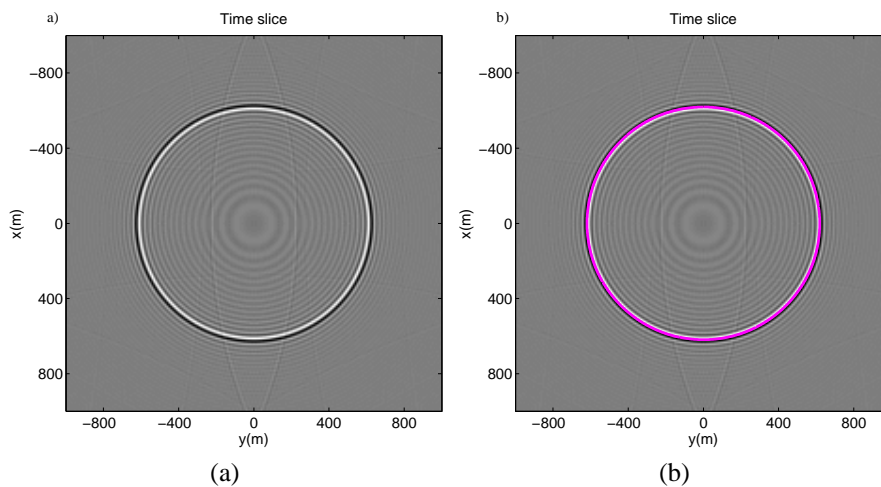
FIG. 18: Time slices of the extrapolated SV wavefield through the same model as ones shown in Figure 17. The authentication of the proposed modelling is shown in (a) and (b) dynamically and kinematically, respectively. The obtained circle illustrate that anisotropy does not have a considerable effect on SV wave propagation.

show the time slices of the SV wavefield extrapolated through a medium characterized by Thomson's parameters shown in appendix and possesses positive ϵ and δ with condition $(\epsilon > \delta)$. In continuation of this, another model possesses the same condition as outlined previously but with large magnitude of Thomson's parameters is taken into account too for observing the effect of anisotropy. By inspecting Figures 19 and 20, it can be revealed that as long as Thomson's parameters follow the condition $(\epsilon > \delta)$ anisotropy does not have a

considerable effect on SV wave propagation either kinematically or dynamically. However, the effect of anisotropy on SV wave propagation can be seen in Figures 21, 22 and 23.
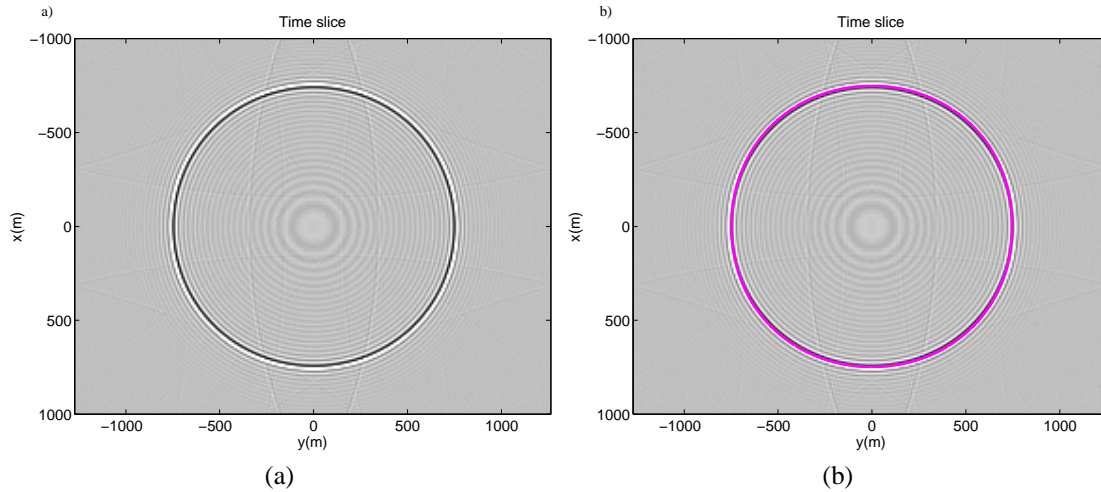
FIG. 19: Time slices of the extrapolated SV wavefield through model 2 ($\epsilon > \delta$) as ones shown in Table 2. The authentication of the proposed modelling is shown as analytic curve overlays with obtained one as shown in (a) and (b). There is no effect of anisotropy for this model.
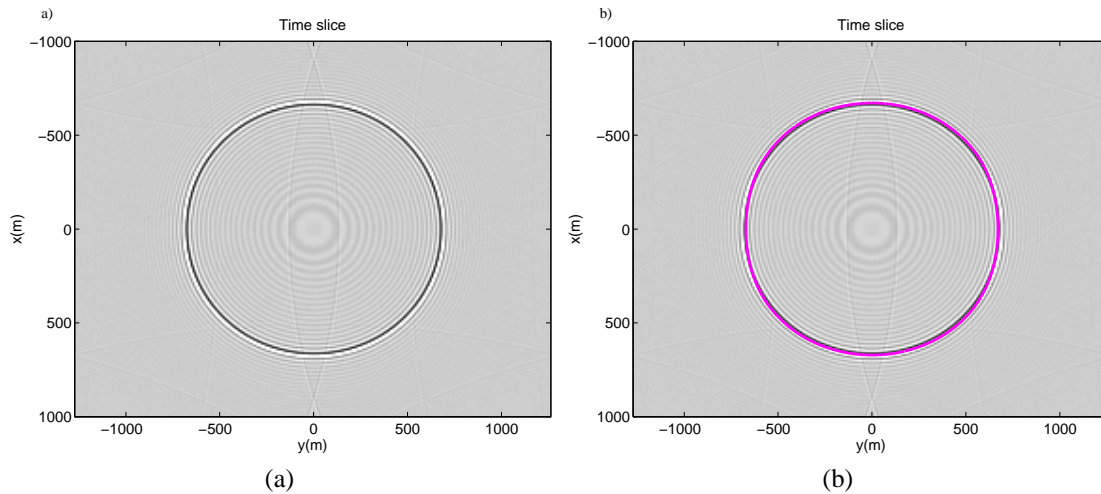
FIG. 20: Time slices (a) and (b) of the extrapolated SV wavefield through model 3 with large magnitude of ($\epsilon > \delta$) shown in Table 2. The authentication of the proposed modelling is shown in (b),kinematically. Still no effect of anisotropy is observed.

Although, the authentication of the proposed modelling, kinematically, is not demonstrated in these cases as obtained results are not matching with analytic curves, it is possible to make some remarkable conclusion as follows

- if ($\epsilon - \delta < 0$), the cusps occur in the in-line direction and can be observed in Figure 21a and be authenticate by Figure 21b.

- if δ is negative and $(\epsilon - \delta > 0)$, the cusps occur near to $45°$ angle from the axis of symmetry. This phenomena is noticed in Figures 22 and 23.
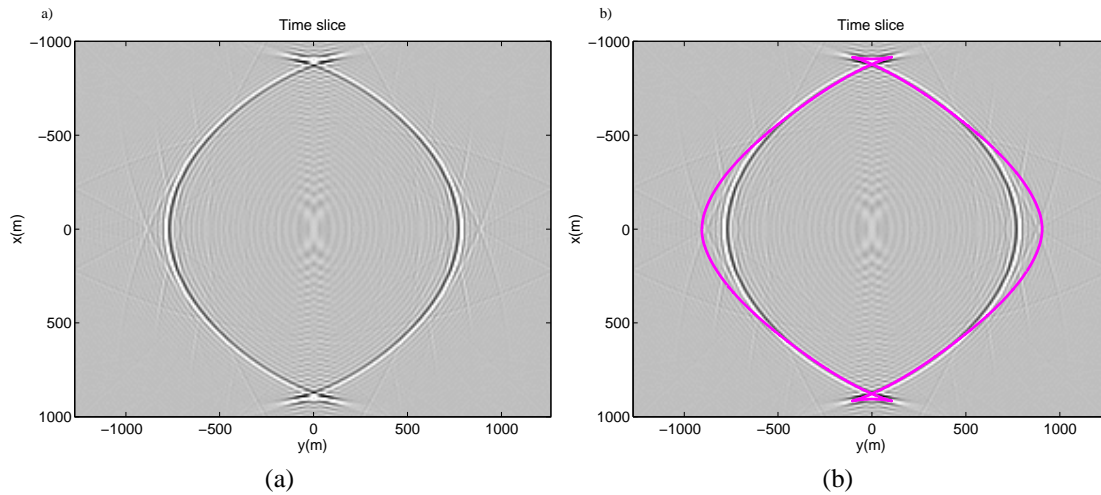
FIG. 21: Time slices of the extrapolated SV wavefield through the model 4 $(\epsilon < \delta)$ shown in Table 2. The cusps phenomena is occurred in the in-line direction. The occurrence of cusps is endorsed by the analytic curve but no overlapping of analytic curve with obtained one is noticed.
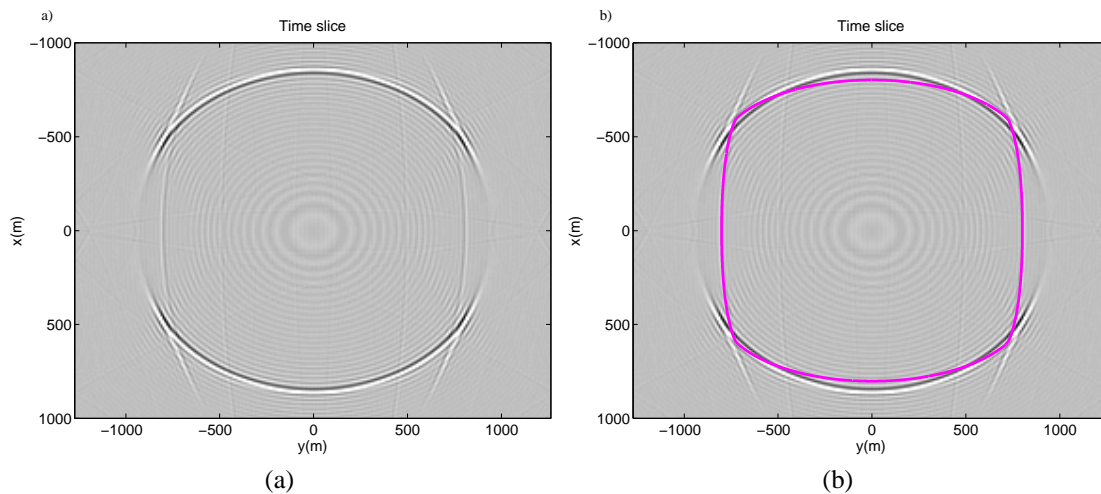
FIG. 22: Time slices of the extrapolated SV wavefield through model 5 $(-\delta)$ shown in Table 2. The cusps is observed near to $45°$.

CONCLUSIONS

We have presented multicomponent modelling of P-wave in plane wave domain for HTI media. The authentication of the proposed phase shift modelling has been demonstrated kinematically and dynamically. Further, the kinematic and dynamic effect of anisotropy on the seismic waves propagation has been demonstrated and the dependency of this analysis on the magnitude of Thomson's parameters is also illustrated. Since the fractures have an impact on the amplitude and travel time of seismic waves propagation, the careful investigation of this impact can be used for fracture detection.
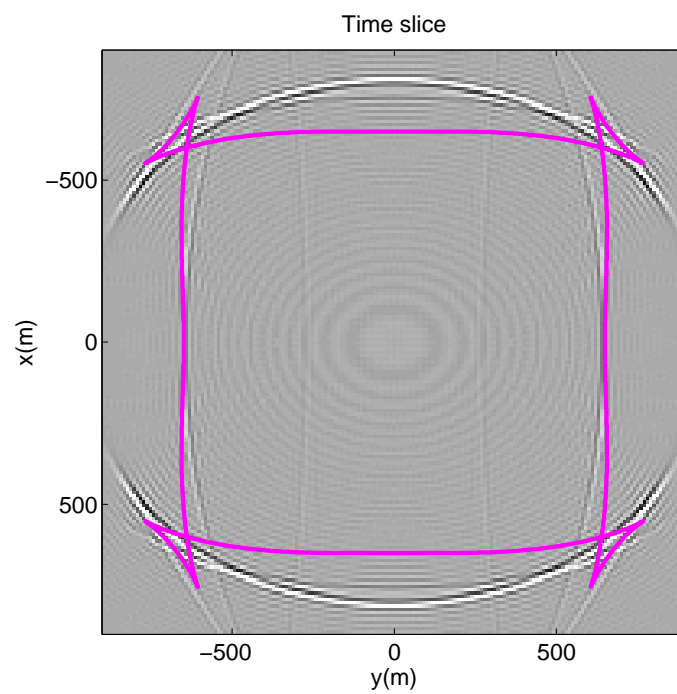
FIG. 23: Time slices of the extrapolated SV wavefield through the model possesses large negative value of δ (model 6) as shown in Table 2.

REFERENCES

Grechka, V., 2009, Application of Seismic Anisotropy in the Oil and Gas Industry.: EAGE.

Larry, L., 2004, Fundamental of Geophysical Interpretation: Society of exploration geophysicists.

Nadri, D., 2009, Non linear estimation of thomson's parameters in transversely isotropic media.: CSIRO Petroleum Resources, –.

Peter, C., L, and Crampin, S., 1990, Seismic fracture anisotropy in the earth crust: An overveiw: Journal of Geophysical Research., **95**.

Sharma, R. K., and Ferguson, R. J., 2010, 9c-3d modeling for vti media.: CREWES Research Report, **22**.

Slawinski, M. A., 2003, Seismic waves and Rays in Elastic Media.: Pergamon Second Edition.

Thomsen, L., 1986, Weak elastic anisotropy: Geophysics, **51**, 1954–1966.

Tsvankin, I., 2001, Seismic Signatures and Analysis of Reflection data in Anisotropic Media.: Handbook of Geophysical Exploration Series.

Xiang-Yangi, L., 1997, Fractured reservoir delineation using multicomponet seismic data.: Geophysical Prospecting, **45**.

Zheng, X., 2006, Seismic azimuthal anisotropy and fracture analysis from p-p reflection data.: M.Sc. thesis, Univ. of Calgary.

APPENDIX

Using the Thomson's parameters, the following relationship between elastic stiffness constant and Thomson's parameters can be established as

$$c_{11} = \rho \alpha_0^2 (1 + 2\epsilon), \tag{A-1}$$

$$c_{33} = \rho \alpha_0^2, \tag{A-2}$$

$$c_{44} = \rho \beta_0^2, \tag{A-3}$$

$$c_{55} = \rho \beta_0^2, \tag{A-4}$$

$$c_{13} = \rho \sqrt{\left(\alpha_0{}^2 - \beta_0{}^2\right)\left((2\delta + 1)\alpha_0{}^2 - \beta_0{}^2\right)} - \rho \beta_0{}^2. \tag{A-5}$$

For given Thomson's parameters, the elastic stiffness constant can be obtained using above equations. As it's known that the elastic stiffness constant remains real for all physical situations, the obtained value of the elastic stiffness constant c_{13} is complex and violates the physical behavior of the elastic stiffness constants for the large negative value of δ. Thus, this condition leads to the unexpected behavior of the wavefield kinematically as well as dynamically.

α_0	β_0	ϵ	δ	γ
2950	1990	0.17	0.09	.14

Table 1: Thomson's Parameters of a medium considered for P and SH waves propagation.

Model	α_0	β_0	ϵ	δ	γ
1	2950	1990	0.17	0.09	.14
2	3600	2000	0.14	0.08	0.16
3	3340	1860	0.49	0.30	0.59
4	3300	2300	0.58	0.84	0.39
5	3600	2100	0.36	-0.08	0.38
6	3377	1490	0.200	-0.282	0.510

Table 2: Thomson's Parameters of models considered for SV wave propagation.